



Applied Mathematics and Nonlinear Sciences

<http://journals.up4sciences.org>

On the stabilizing effect of chemotaxis on bacterial aggregation patterns

J. Alejandro Butanda¹, Carlos Málaga², Ramón G. Plaza^{3†}

¹Centro de Investigación en Matemáticas A. C., Jalisco s/n, La Valenciana, C.P. 36023 Guanajuato, Gto., MEXICO

²Departamento de Física, Facultad de Ciencias, Universidad Nacional Autónoma de México, Circuito Exterior s/n, Ciudad Universitaria, C.P. 04510 Cd. de México, MEXICO

³Instituto de Investigaciones en Matemáticas Aplicadas y en Sistemas, Universidad Nacional Autónoma de México, Circuito Escolar s/n, Ciudad Universitaria, C.P. 04510 Cd. de México, MEXICO

Submission Info

Communicated by Tomás Caraballo
Received 5th February 2017
Accepted 16th May 2017
Available online 16th May 2017

Abstract

We consider a chemotaxis-reaction-diffusion system that models the dynamics of colonies of *Bacillus subtilis* on thin agar plates. The system of equations was proposed by Leyva *et al.* [14], based on a previous non-chemotactic model by Kawasaki and collaborators [9], which reproduces the dense branching patterns observed experimentally in the semi-solid agar, low-nutrient regime. Numerical simulations show that, when the chemotactic sensitivity toward nutrients is increased, the morphology of the colony changes from a dense branched pattern to a uniform envelope that propagates outward. Here, we provide a quantitative argument that explains this change in morphology. This result is based on energy estimates on the spectral equations for perturbations around the envelope front, suggesting the suppression of colony branching as a result of the stabilizing effect of the increasing chemotactic signal.

Keywords: Nutrient chemotaxis; non-linear cross diffusion; stability of fronts.

AMS 2010 codes: 92C17, 92D25, 35B35, 35C07.

1 Introduction

When grown on semi-solid agar surfaces, many species of bacteria exhibit a variety of complex spatial patterns which depend upon certain environmental conditions, such as the level of nutrients, the hardness of the agar substrate and the temperature. For instance, when concentrations of the bacterium *Bacillus subtilis* are

†Corresponding author.

Email address: plaza@mym.iimas.unam.mx

inoculated on a moderately soft agar plate with poor nutrient levels, the bacteria form dense branching colonies with a smooth envelope propagating outward (cf. Ohgiwari *et al.* [18]). If the nutrient level is increased and the agar is softer, then the bacteria form simple circular patterns growing in an homogeneous fashion (cf. Wakita *et al.* [24]).

Continuous deterministic reaction-diffusion systems of equations for the bacterial density and the nutrient concentration appear to be good models for the transition from a dense branch morphology (DBM) regime to the homogeneous envelope front type of pattern (see, e.g., [3, 5, 9, 14, 21]). In the mid nineties, Kawasaki *et al.* [9] proposed a reaction diffusion model with a non-linear, degenerate, density-dependent, cross-diffusion coefficient, which captures many of the main features of the patterns of *B. subtilis* found experimentally. Since many aspects of the observed patterns can only be understood if one takes into account the effects of chemotaxis (that is, the tendency of some biological individuals to move preferably toward higher concentrations of chemicals [1, 23]), in a recent contribution Leyva *et al.* [14] proposed a chemotactic version of the original model by Kawasaki and collaborators, which incorporates a chemotactic toward nutrient concentration term into the equations. This new term is appropriately adapted to the cross diffusion coefficient under consideration, that is, it follows an empirical rule suggested by Ben-Jacob and his group [3, 8] (see section 2.1 below). In [14], the authors present the outcome of numerical simulations and observed that the colony envelope moves faster if the chemotactic signal is present. Moreover, they perform asymptotic estimations on the normal speed of the front as a function of the chemotactic sensitivity. In addition, simulations in the soft-agar, low-nutrient regime indicate a change of morphology from a DBM-like pattern to an homogeneous circular front when the chemotactic signal is increased.

In this paper we provide a quantitative estimation that explains, at first order approximation, this change in morphology. More precisely, we show that when the chemotactic sensitivity is increased, the eigenvalues of the linearized operator around the envelope front become more stable (that is, they move to the stable complex half plane), suggesting, in this fashion, that the homogeneous front is more difficult to destabilize. This mechanism seems to suppress the branching of the colony when the chemotactic signal toward nutrient is stronger. For that purpose, we make some approximations, which include the derivation of an effective scalar equation for the bacterial density (thanks to the balanced production of bacteria and consumption of nutrient), and the approximation of a smooth envelope front by a locally planar traveling front (cf. [7]). We employ energy estimates at the level of the resulting spectral equations which show that the front is spectrally stable under transversal perturbations. These estimates generalize previous calculations for systems with constant diffusion coefficients [2, 4], and make use of recently developed techniques to locate point spectra for stability problems with density-dependent, degenerate diffusivities [15].

The rest of the paper is organized as follows. In section 2 we present the model in [14] and show some particular numerical simulations that exhibit the change in morphology when chemotaxis is switched on. The central section 3 contains the energy estimates, performed on a generic model after proper approximations, which yield the transversal spectral stability of the front, as well as the energy bounds for the eigenvalues in terms of the chemotactic signal. The final section 4 contains a brief discussion on our (and related) results.

2 The effects of chemotaxis on bacterial aggregation dynamics

In this section we describe in detail a chemotaxis-reaction-diffusion model for bacterial growth, which includes a nonlinear, cross-diffusion term, as well as a chemotactic term toward nutrient. We also present the results of numerical simulations of this system in the DBM-regime, which keep the environmental conditions fixed whereas the chemotactic parameter is increased.

2.1 Chemotactic non-linear degenerate cross-diffusion model

Based on the model by Kawasaki *et al.* [9], Leyva and collaborators [14] have proposed the following chemotactic, non-linear degenerate cross-diffusion system of equations in order to model the dynamics of *B. subtilis* on thin agar plates:

$$\begin{aligned} u_t &= \nabla \cdot (\sigma uv \nabla u) - \nabla \cdot (\xi(u, v) \chi(v) \nabla v) + \theta \kappa uv, \\ v_t &= D_v \Delta v - \kappa uv, \end{aligned} \quad (1)$$

for $(x, y) \in \Omega \subset \mathbb{R}^2$, $t \in (0, +\infty)$. Here Ω is an open, bounded spatial domain and $t > 0$ denotes time. Scalar functions $v = v(x, y, t)$ and $u = u(x, y, t)$ represent the concentration of nutrients and the density of bacterial cells, respectively. Moreover, $\kappa > 0$ is a positive constant and $\theta > 0$ is the constant conversion factor.

The constant $D_v > 0$ is the diffusion coefficient for the nutrient, whereas the diffusion coefficient of bacteria is a non-linear function of the concentrations, as proposed by Kawasaki *et al.* [9],

$$D_u = D_u(u, v) = \sigma uv, \quad (2)$$

where $\sigma > 0$ measures the hardness of the agar substrate. This nonlinear diffusion coefficient was proposed to model the experimental observations by Oghiwari *et al.* [18], which suggest that bacteria are immotile when either the bacterial density u or the nutrient concentration v are low, and become active as u or v increase.

The chemotactic sensitivity function $\chi = \chi(v)$ follows a Lapidus-Schiller receptor law [13]:

$$\chi(v) = \frac{\chi_0 K_d}{(K_d + v)^2}; \quad (3)$$

here $\chi_0 > 0$ is a constant, measuring the strength of the chemotactic signal, and $K_d > 0$ is the receptor-ligand binding dissociation constant (measured in nutrient concentration units), representing the nutrient level needed for half receptor to be occupied. It depends on the bacterial species under consideration, alone. Finally, the bacterial response function $\xi = \xi(u, v)$, which must be non-negative for attractive chemotaxis, measures the sensitivity of the bacteria to the effective sensed gradient, namely $\chi(v) \nabla v$, and it has the same units as a diffusion coefficient. In the DBM-regime of soft agar and nutrient poor medium, Leyva *et al.* [14] proposed the following bacterial response function:

$$\xi(u, v) = u D_u(u, v) = \sigma u^2 v. \quad (4)$$

This choice obeys the empiric law proposed by E. Ben-Jacob and his group [3, 8] which states that the bacterial response function should be proportional to the product of the bacterial density and its diffusion coefficient:

$$|\xi| \propto u D_u. \quad (5)$$

The explanation by Ben-Jacob and collaborators goes as follows. Bacterial motion is, necessarily, cooperative at low bacterial densities. This can be roughly modeled by taking the diffusion coefficient to be dependent on bacterial density. Thus, the chemotactic flux should be modified accordingly as $J_{\text{chem}} = -\xi(u, v) \chi(v) \nabla v$, where ξ follows the empirical rule (5). Notice that when the diffusion coefficient is constant, $D_u(u, v) = 1$ (after normalizations), then the bacterial response function is $\xi = u$, recovering the standard Keller-Segel [10, 11] chemotactic flux: $J_{\text{chem}} = -u \chi(v) \nabla v$.

System (1) is further endowed with initial conditions of the form

$$u(x, y, 0) = u_0(x, y), \quad (x, y) \in \Omega, \quad (6a)$$

$$v(x, y, 0) = v_0, \quad \text{constant}, \quad (6b)$$

where $v_0 > 0$ is the uniform initial distribution of nutrient, and the function $u_0 = u_0(x, y)$ is the initial inoculation of bacteria in Ω (for example, a localized Gaussian distribution). In addition, we impose no-flux or Neumann boundary conditions,

$$\nabla u \cdot \mathbf{n} = 0 \quad \text{and} \quad \nabla v \cdot \mathbf{n} = 0, \quad \text{at } \partial\Omega, \quad (7)$$

where $\mathbf{v} \in \mathbb{R}^2$, $|\mathbf{v}| = 1$, is the unit outer normal at each point of $\partial\Omega$.

After an appropriate scaling of variables (see [14] for details), system (1) can be put in non-dimensional form,

$$\begin{aligned} u_t &= \sigma_0(1 + \hat{\Delta})\nabla \cdot (uv\nabla v) - \chi_0\sigma_0(1 + \hat{\Delta})\nabla \cdot \left(\frac{u^2v}{(1+v)^2}\nabla v \right) + uv, \\ v_t &= \Delta v - uv, \end{aligned} \quad (8)$$

after suitable modifications for the functions D , ξ and χ (with a slight abuse of notation, we use the same letters for all functions and independent variables). Following Kawasaki *et al.* [9] (see also [14]), and in order to avoid intrinsic symmetries in the bacterial patterns induced by numerical discretization, in (8) we have considered

$$D(u, v) = \sigma uv = \sigma_0(1 + \hat{\Delta})uv, \quad (9)$$

where $\sigma_0 > 0$ is a non-dimensional constant, and $\hat{\Delta}$ is a stochastic fluctuation. Whence, after the scaling, the only non-dimensional free parameters are $\sigma_0 > 0$, which measures the hardness of the agar substrate (larger values of σ_0 for lower agar concentrations); $\chi_0 \geq 0$, which measures the strength of the chemotactic signal; and $v_0 > 0$, the relative initial concentration of nutrient.

2.2 Numerical simulations

We now present the results of numerical simulations of system (8), subject to boundary conditions of Neumann type (7), and with initial conditions of form (6a) and (6b). The calculations were performed in a two-dimensional square domain

$$\Omega = (-L/2, L/2) \times (-L/2, L/2),$$

with center at the origin, and sides of length $L = 680$. We employed an explicit Runge-Kutta time stepper and finite differences scheme, on a spatial square grid of $N = 4096$ points. Thus, the discretization mesh width was taken as $\Delta x = \Delta y = L/N \approx 0.166$. The time step size considered was $\Delta t = 0.011$, for which the method is stable.

For the sake of comparison with the numerical simulations in [9, 14], the initial distribution of bacterial cell density was of Gaussian type, centered at the origin,

$$u_0(x, y) = u_M e^{-(x^2+y^2)/6.25},$$

where $u_M = 0.71$ is the maximum density at the center. The uniform initial distribution of nutrient was taken as

$$v_0(x, y) \equiv v_0 = 0.71,$$

as considered in Kawasaki *et al.* [9]. The coefficient $\sigma > 0$, that appears in the diffusion for bacteria, was perturbed from a mean value $\sigma_0 > 0$ via a stochastic fluctuation $\hat{\Delta}$, following (9). The value for the non-dimensional parameter σ_0 was taken as $\sigma_0 = 4.0$, measuring the softness/hardness of the agar substrate. These parameter values ($v_0 = 0.71$, $\sigma_0 = 4.0$) correspond to an environment with semi-solid agar (soft medium) and low-to-medium concentration of nutrients, where DBM patterns arise, characterized by smooth envelope fronts moving outward. In the absence of chemotaxis (cf. [9, 14]), these conditions produce dense branches (fingering) and ramified patterns.

While fixing these conditions for nutrient and agar substrate, we switched on the chemotactic parameter $\chi_0 \geq 0$. We performed simulations for different parameter values of the chemotactic sensitivity χ_0 . The results of the simulations can be observed in Figure 1. A sequence of three time steps (in rows) of the contour plots for the computed bacterial density are presented. The numerical values for $v_0 = 0.71$ and $\sigma_0 = 4.0$ are kept fixed in the simulations, whereas, in columns, the values for the chemotactic sensitivity are varied and taken as $\chi_0 = 0$, 2.5 and 5.0, respectively. Notice the appearance of a colony envelope front for u , moving outward as time goes by.

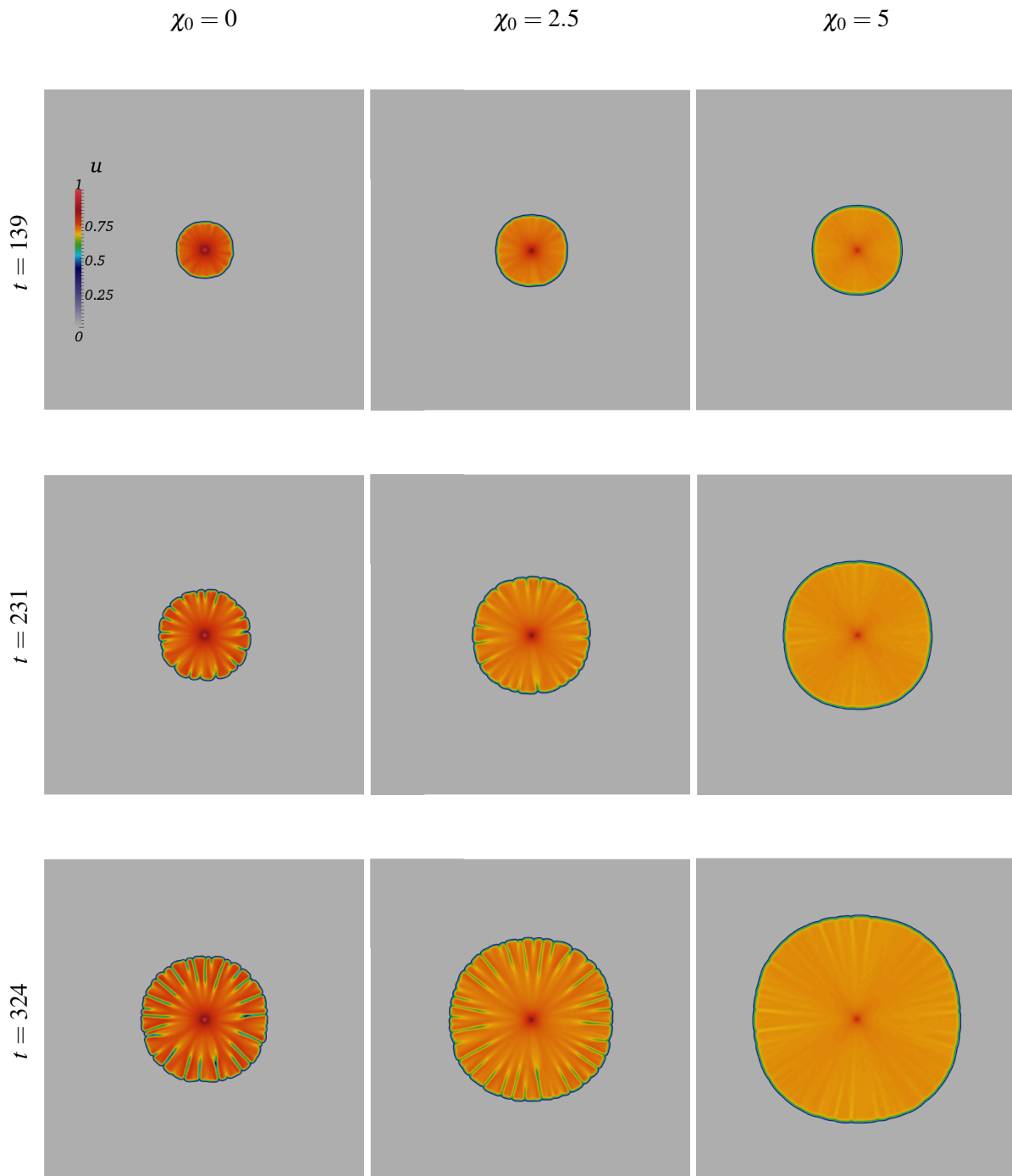


Fig. 1 A sequence of three time steps, in rows, of the contour plots of u computed numerically, for three values of χ_0 , in columns, showing the change of morphology in the bacterial patterns. Notice the stabilizing effect of chemotaxis on the bacteria envelope front.

The first apparent change with respect to absent or weak chemotaxis is that the colony envelope front moves faster outward, as the chemotaxis is increased. This expected behavior has been already quantified in [14], where estimates on the normal speed of the front in terms of the chemotactic signal were established. The other significant change is morphological. Notice that the envelope front goes from a branched (dendrite-like) pattern ($\chi_0 = 0$) to a more homogeneous bacterial pattern ($\chi_0 = 5.0$), in which the protuberances seem to disappear.

Apparently, the increase in the chemotactic signal produces a transition from the DBM-morphology to the homogeneous disk type morphology which is observed in soft-agar, high-nutrient regimes [3, 9]. The presence of the chemotactic signal seems to suppress the onset of instability that causes the formation of branches. This behaviour was already noticed in the simulations performed by Leyva *et al.* [14]. However, the authors did not provide any justification of this sudden change in morphology of the patterns.

3 Transversal stability

In this section, we provide a quantitative argument that justifies the change in morphology experienced by the bacterial colony as the intensity of the chemotactic signal is increased, under the same conditions on motility and level of nutrient. For that purpose, let us consider the following generic chemotactic cross-diffusion model:

$$\begin{aligned} u_t &= \nabla \cdot (\bar{D}(u, v) \nabla u) - \nabla \cdot (\xi(u, v) \chi(v) \nabla v) + uv, \\ v_t &= \Delta v - uv, \end{aligned} \quad (10)$$

written in appropriate non-dimensional variables.

In the sequel, we make the following assumptions:

(H1) $\bar{D} \in C^2(\mathbb{R}^2)$, $\bar{D}(u, v) \geq 0$ for all $u, v \in \mathbb{R}$. Moreover, $\bar{D} = 0$ if $u = 0$ or $v = 0$.

(H2) For all $u, v \in \mathbb{R}$ under consideration:

$$\xi(u, v) = u \bar{D}(u, v).$$

(H3) $\chi \in C^2(\mathbb{R})$ and uniformly bounded: $0 \leq \chi(v) \leq C$ for some constant $C > 0$ and all $v \in \mathbb{R}$ under consideration.

Hypothesis (H1) generalizes the nonlinear degenerate diffusion function of Kawasaki *et al.* [9], given by (2). It is degenerate at $u = 0$ or $v = 0$, when either the nutrient or the bacterial density vanishes. Hypothesis (H2) simply expresses that the bacterial response function should satisfy (5), as proposed by Ben-Jacob in the DBM-regime [3, 8]. Finally, hypothesis (H3) resembles a receptor-ligand chemotactic signal, which should be bounded thanks to the saturation of receptors, just like the Lapidus-Schiller receptor law (3). Under these assumptions, the chemotactic signal is attractive.

Notice that the kinetic terms in system (10) are of the form $\pm f(u, v) = \pm uv$, that is, there is a balance between the production term for bacterial density, and the loss of nutrient concentration. The product uv measures the probability of encounters of bacterial cells with the nutrient.

3.1 Approximations

In order to quantify the effects of chemotaxis on the branching patterns, we are going to make some approximations on the solutions to system (10). First, we employ the reduction suggested by Kawasaki *et al.* [9]. They observed that, due to the form of the reaction terms (production and loss terms are balanced), in the absence of diffusion the total mass is approximately conserved for small values of nutrient and bacterial density. In our model, if we neglect both diffusion and chemotaxis (the latter is also vanishing thanks to the bacterial response under consideration –hypothesis (H3)–), then we add the equations and integrate in time to obtain

$$u + v \approx C, \quad \text{constant.}$$

This constant can be taken as $C = v_0$, the initial nutrient reference value. This approximation is consistent with the numerical simulations of [9] (in the absence of chemotactic signal), and those of [14], where chemotaxis is incorporated. Such simulations show that, at first order, u is constant inside the envelope front and v is near zero (total consumption of resources), whereas away from the front $u = 0$ and the nutrient is not yet consumed. Thus, we make the following approximation

$$v = v_0 - u. \tag{11}$$

Upon substitution into system (10) one obtains a scalar equation for the bacterial density of the form

$$u_t = \nabla \cdot (D(u)\nabla u) + g(u), \tag{12}$$

where the effective nonlinear, degenerate, density-dependent diffusion coefficient is given by

$$D(u) := \bar{D}(u, v_0 - u)(1 + u\chi(v_0 - u)), \tag{13}$$

and the effective reaction term is

$$g(u) := v_0 u \left(1 - \frac{u}{v_0}\right). \tag{14}$$

It is to be observed that, under the hypothesis of attractive chemotaxis towards nutrients (H3), the effective diffusion coefficient is a non-negative, density-dependent nonlinear function. Moreover, it is doubly-degenerate, in the sense that it vanishes at $u = 0$ and at $u = v_0$ (equivalently, at $v = 0$). In addition, notice that the resulting reaction term (14) is of Fisher-KPP (or logistic) type [6, 12].

Finally, since $\chi(\cdot)$ is a C^2 function near $v = 0$, we approximate χ by a constant value,

$$\chi(v) \equiv \chi(0) = \chi_0 \geq 0,$$

that is, we assume that the chemotactic sensitivity does not vary for v near zero. This simplification allows us to work with the parameter $\chi_0 \geq 0$ of the numerical simulations as a measure of the chemotactic signal, which can be switched on and off. Since for suitably normalized values of $v \in [0, v_0]$ the Lapidus-Schiller chemotactic law is uniformly bounded, this approximation represents no loss of generality.

3.2 Perturbations of the envelope front

Following Funaki *et al.* [7], we assume that, locally, the envelope front behaves like a planar front, and that its propagation happens in one preferred direction. Thus, let us consider an approximated one-dimensional planar front solution of the form

$$u(x, y, t) = \phi(x - ct) = \phi(z),$$

on a strip domain,

$$\Omega_L = \{(x, y) \in \mathbb{R}^2 : -\infty < x < \infty, 0 < y < L\},$$

for some $L > 0$. Here $z := x - ct$ denotes the (Galilean) variable of translation, and $c \in \mathbb{R}$ is the constant speed of the front. Substituting the traveling front solution into (12) we obtain the following ordinary differential equation for the profile function ϕ ,

$$-c\phi_z = D(\phi)\phi_{zz} + D(\phi)_z\phi_z + g(\phi). \tag{15}$$

In pattern formation problems, it is natural to consider infinite domains and to neglect the influence of boundary conditions. Due to finite speed of propagation and the fact that we are interested in the local-in-time, local-in-space evolution near the interface of the envelope front, working on an infinite domain Ω_L means no loss of generality. Consequently, we assume that the front has asymptotic limits of the form

$$u_{\pm} = \lim_{z \rightarrow \pm\infty} \phi(z).$$

Since the front spreads from the region occupied by the cells toward outer regions filled with nutrient, we consider

$$u_+ = 0, \quad u_- = v_0.$$

Moreover, we shall assume that the front is monotone, that is,

$$\phi_z(z) < 0, \quad \text{for all } z \in \mathbb{R}. \tag{16}$$

Remark 1. The existence of traveling fronts for reaction diffusion equations where the diffusion coefficient is density-dependent and degenerate, and the reaction term is of Fisher-KPP type, as well as its monotonicity properties, have been addressed in the literature by several authors; see, for example, [16, 19]. As a by-product of the existence analysis of fronts for degenerate diffusion coefficients, which decay to zero as they approach equilibria,

$$D(\phi) \rightarrow 0, \quad \text{as } \phi(z) \rightarrow \begin{cases} 0, & z \rightarrow +\infty \\ v_0, & z \rightarrow -\infty, \end{cases}$$

it turns out that the heteroclinic orbit belongs to a center manifold passing through the degenerate equilibrium points. For instance, when $\phi(z) \rightarrow 0$ as $z \rightarrow +\infty$, the center manifold on the phase plane looks like [19, 20],

$$\phi_z = -\alpha\phi + O(\phi^2),$$

for some constant $\alpha > 0$, from which we can deduce the exponential decay of ϕ and its derivatives,

$$|\phi|, |\phi_z|, |\phi_{zz}| \leq Ce^{-\alpha z}, \quad z \rightarrow +\infty, \tag{17}$$

as well as the rate of decay of the diffusion coefficient

$$D(\phi) = D'(0)\phi + \frac{1}{2}D''(0)\phi^2 + \dots = O(\phi) \leq Ce^{-\alpha z}, \tag{18}$$

for $\phi \sim 0$. Similar decay rates hold at the other degenerate point, as $\phi \rightarrow v_0$ when $z \rightarrow -\infty$. See [15, 16, 19, 20] for further information.

Let us consider perturbations of the form $w = w(z, y, t)$, satisfying the boundary conditions

$$\left. \begin{aligned} w(\pm\infty, y, t) &= 0, & t > 0, \quad 0 < y < L, \\ w(z, L, t) = w(z, 0, t) &= 0, & t > 0, \quad z \in \mathbb{R}. \end{aligned} \right\} \tag{19}$$

Substituting $u(x, y, t) = \phi(z) + w(z, y, t)$ into (12) and expanding the nonlinear functions we obtain

$$\begin{aligned} -c\phi_z - cw_z + w_t &= D(\phi)(w_{zz} + w_{yy}) + (D(\phi)\phi_z)_z + 2D(\phi)_z w_z + D(\phi)_{zz} w + \\ &+ g(\phi) + g'(\phi)w + O(|w|^2 + |w||\nabla w|). \end{aligned}$$

In view of the profile equation (15) and linearizing around the front, one arrives at the following linear equation for the perturbation

$$w_t = D(\phi)(w_{zz} + w_{yy}) + (2D(\phi)_z + c)w_z + (D(\phi)_{zz} + g'(\phi))w. \tag{20}$$

In order to establish the associated spectral problem, let us specialize (20) to solutions of the form

$$w(z, y, t) = e^{\lambda t} U(z, y),$$

where $\lambda \in \mathbb{C}$ and $U \in L^2(\Omega_L)$, subject to the following boundary conditions

$$\left. \begin{aligned} U(\pm\infty, y) &= 0, & y \in [0, L], \\ U_y(z, 0) = U_y(z, L) &= 0, & z \in \mathbb{R}. \end{aligned} \right\} \tag{21}$$

Substituting into (20) we obtain the following spectral problem,

$$\lambda U = D(\phi)(U_{zz} + U_{yy}) + (2D(\phi)_z + c)U_z + (D(\phi)_{zz} + g'(\phi))U, \quad (22)$$

where $\lambda \in \mathbb{C}$ plays the role of an eigenvalue, and $U \in L^2(\Omega_L)$ is the associated eigenfunction. The right hand side of (22) defines a closed, densely defined operator in $L^2(\Omega_L)$, namely

$$\begin{aligned} \mathcal{L}U &= D(\phi)(U_{zz} + U_{yy}) + (2D(\phi)_z + c)U_z + (D(\phi)_{zz} + g'(\phi))U, \\ \mathcal{L} : \mathcal{D}(\mathcal{L}) &= H^2(\Omega_L) \subset L^2(\Omega_L) \rightarrow L^2(\Omega_L), \end{aligned}$$

with domain $\mathcal{D}(\mathcal{L}) = H^2(\Omega_L)$. \mathcal{L} is the linearized operator around the front. For any $U \in L^2(\Omega_L)$ satisfying (21) and any $m = 0, 1, 2, \dots$, let us define

$$U_m(z) := \int_0^L U(z, y) Y_m(y) dy,$$

where

$$Y_m(y) = \begin{cases} \frac{1}{\sqrt{L}}, & m = 0, \\ \sqrt{\frac{2}{L}} \cos\left(\frac{m\pi y}{L}\right), & m = 1, 2, \dots \end{cases}$$

Eigenfunctions are thus decomposed as

$$U(z, y) = \sum_{m=0}^{+\infty} U_m(z) Y_m(y).$$

Substituting into (22) and collecting equal modes for each $m \in \mathbb{Z}, m \geq 0$, we establish the following hierarchy of spectral equations,

$$\lambda U_0 = D(\phi)\partial_z^2 U_0 + (2D(\phi)_z + c)\partial_z U_0 + (D(\phi)_{zz} + g'(\phi))U_0, \quad \text{for } m = 0, \quad (23)$$

and,

$$\lambda U_m = D(\phi)\partial_z^2 U_m + (2D(\phi)_z + c)\partial_z U_m + \left(D(\phi)_{zz} + g'(\phi) - \frac{m^2\pi^2}{L^2}D(\phi)\right)U_m, \quad \text{for } m \in \mathbb{Z}, m \geq 1, \quad (24)$$

for the same eigenvalue $\lambda \in \mathbb{C}$. We are interested in solutions $U_m \in L^2(\mathbb{R})$ to (23) and (24), for all $m \geq 0$. The right hand sides of both equations are closed, densely defined differential operators of second order in $L^2(\mathbb{R})$, with domain $H^2(\mathbb{R})$.

Remark 2. Observe that, in view of the profile equation (15), the function $\Phi := \phi_z \in H^2(\mathbb{R})$ is a solution to (23) with $\lambda = 0$ and $m = 0$. Indeed, if we differentiate (15) we obtain

$$0 = D(\phi)\Phi_{zz} + (2D(\phi)_z + c)\Phi_z + (D(\phi)_{zz} + g'(\phi))\Phi.$$

This shows that $\lambda = 0$ is an eigenvalue (associated to translation) of (22) with eigenfunction $U(z, y) = \Phi(z) = \phi_z(z)$. Clearly, its expansion is given by $U_0 = \sqrt{L}\phi_z$, and

$$U_m(z) = \int_0^L \phi_z(z) Y_m(y) dy = 0,$$

for all $m \geq 1$, in that case.

3.3 Energy estimates and transversal stability

Following [15], for each mode $m \in \mathbb{Z}$, $m \geq 0$, let us define the change of variables

$$W_m(z) := U_m(z) \exp\left(\frac{c}{2} \int_{z_0}^z \frac{d\zeta}{D(\phi(\zeta))}\right),$$

where $z_0 \in \mathbb{R}$ is fixed but arbitrary. Let us suppose that the eigenfunction $U \in H^2(\Omega_L) \subset L^2(\Omega_L)$ decays sufficiently fast to zero as $z \rightarrow \pm\infty$ so that, for each $m \geq 1$,

$$W_m \in H^2(\mathbb{R}).$$

Remark 3. This assumption simply implies that we restrict the analysis to the set of localized perturbations that decay fast enough. At the level of the spectral problem, by a standard cut-off argument one can always approximate any generic localized perturbation by rapidly decaying ones; at the level of the evolution equations, we are simply restricting the space of controlled perturbations to a smaller space with fast decay.

Hence, we can compute

$$\begin{aligned} \partial_z U_m &= \exp\left(\frac{c}{2} \int_{z_0}^z \frac{d\zeta}{D(\phi(\zeta))}\right) \left(\partial_z W_m - \frac{c}{2D(\phi)} W_m\right), \\ \partial_z^2 U_m &= \exp\left(\frac{c}{2} \int_{z_0}^z \frac{d\zeta}{D(\phi(\zeta))}\right) \left(\partial_z^2 W_m - \frac{c}{2D(\phi)} \partial_z W_m + \left(\frac{cD(\phi)_z}{2D(\phi)^2} + \frac{c^2}{4D(\phi)^2}\right) W_m\right), \end{aligned}$$

and substitute into the spectral equation (24) to obtain

$$\lambda W_m = D(\phi) \partial_z^2 W_m + 2D(\phi)_z \partial_z W_m + \left(H(z) - \frac{m^2}{\pi^2 L^2} D(\phi)\right) W_m, \tag{25}$$

for all $m \in \mathbb{Z}$, $m \geq 0$ and the eigenvalue $\lambda \in \mathbb{C}$ associated to the perturbation. Here

$$H(z) := D(\phi)_{zz} + g'(\phi) - \frac{c^2}{4D(\phi)} - \frac{cD(\phi)_z}{2D(\phi)}.$$

The following lemma states that any eigenvalue is real and non-positive, that is, the front is *spectrally stable* under transversal perturbations.

Lemma 1. *If $\lambda \in \mathbb{C}$ is an eigenvalue of the associated spectral problem, such that (25) holds for each mode $m \in \mathbb{Z}$, $m \geq 0$ with $W_m \in H^2(\mathbb{R})$, then $\lambda \in \mathbb{R}$ and $\lambda \leq 0$.*

Proof. When $m = 0$ and $\Phi = \phi_z$, the change of variables for this eigenfunction, namely,

$$\Psi(z) := \Phi(z) \exp\left(\frac{c}{2} \int_{z_0}^z \frac{d\zeta}{D(\phi(\zeta))}\right),$$

yields

$$0 = D(\phi) \partial_z^2 \Psi + 2D(\phi)_z \partial_z \Psi + H(z) \Psi. \tag{26}$$

Multiply (26) and (25) by $D(\phi) \geq 0$ and rearrange the terms to obtain

$$\lambda D(\phi) W_m = \partial_z (D(\phi)^2 \partial_z W_m) + D(\phi) H(z) W_m - \frac{m^2}{\pi^2 L^2} D(\phi)^2 W_m, \tag{27}$$

for all $m \geq 1$, and

$$0 = \partial_z (D(\phi)^2 \Psi_z) + D(\phi) H(z) \Psi. \tag{28}$$

Notice that the zero-eigenfunction Φ (and its corresponding transformed eigenfunction Ψ) are independent of the eigenfunction U associated to the eigenvalue λ under consideration. Nonetheless, equation (28) holds, with the same coefficient $H(\cdot)$ as in (27). Whence, from monotonicity of the front (see (16)), we have that $\Phi = \phi_z \neq 0$ and, consequently, $\Psi \neq 0$. Therefore, we can substitute

$$D(\phi)H(z) = -\frac{(D(\phi)^2\Psi_z)_z}{\Psi},$$

into (27) to arrive at

$$\lambda D(\phi)W_m = (D(\phi)^2\partial_z W_m)_z - \left(\frac{D(\phi)^2\Psi_z}{\Psi} + \frac{m^2}{\pi^2 L^2} D(\phi)^2 \right) W_m.$$

Take the L^2 product of W_m with last equation and integrate by parts. The result is

$$\begin{aligned} \lambda \int_{-\infty}^{+\infty} D(\phi)|W_m|^2 dz &= \int_{-\infty}^{+\infty} \bar{W}_m (D(\phi)^2\partial_z W_m)_z dz - \int_{-\infty}^{+\infty} \frac{(D(\phi)^2\Psi_z)_z}{\Psi} |W_m|^2 dz + \\ &\quad - \frac{m^2}{\pi^2 L^2} \int_{-\infty}^{+\infty} D(\phi)^2 |W_m|^2 dz \\ &= \int_{-\infty}^{+\infty} D(\phi)^2 \left(\Psi_z \partial_z \left(\frac{|W_m|^2}{\Psi} \right) - |\partial_z W_m|^2 - \frac{m^2}{\pi^2 L^2} |W_m|^2 \right) dz \\ &= - \int_{-\infty}^{+\infty} D(\phi)^2 \Psi^2 \left| \partial_z \left(\frac{W_m}{\Psi} \right) \right|^2 dz - \frac{m^2}{\pi^2 L^2} \int_{-\infty}^{+\infty} D(\phi)^2 |W_m|^2 dz \\ &\leq 0, \end{aligned} \tag{29}$$

for any $m \geq 1$. We conclude that λ is real and non-positive. \square

Remark 4. Lemma 1 means that, at first order approximation (locally planar front for a scalar equation due to the balanced source and loss kinetic terms), the envelope front is stable under transversal small, local-in-space perturbations. This behaviour is verified by the numerical calculation of the actual (curved) envelope front.

Remark 5. The result of Lemma 1 can be extrapolated to a whole family of operators indexed by the transversal Fourier frequencies. Indeed, if we consider the eigenvalue problem (22) on $L^2(\mathbb{R}^2)$ and eigenfunctions of the form $U = e^{i\xi} W(z)$ with $W \in L^2(\mathbb{R})$ then we obtain the following family of linear operators

$$\begin{aligned} \mathcal{L}_\xi W &= D(\phi)W_{zz} + (2D(\phi)_z + c)W_z + (D(\phi)_{zz} + g'(\phi) - \xi^2 D(\phi))W, \\ \mathcal{L}_\xi : L^2 &\rightarrow L^2, \end{aligned}$$

for each $\xi \in \mathbb{R}$. A similar analysis (under similar decay assumptions) leads to spectral stability of each operator \mathcal{L}_ξ , with $\xi \in \mathbb{R}$ fixed, generalizing in this fashion the observation by Butanda [4] in the constant diffusion case.

3.4 The stabilizing effect of chemotaxis

Let us define

$$\eta(z) := \sqrt{D(\phi(z))} \geq 0, \quad z \in \mathbb{R},$$

and the customary weighted energy function spaces

$$H_\eta^k(\mathbb{R}; \mathbb{C}) = \{v : \eta(z)v(z) \in H^k(\mathbb{R}; \mathbb{C})\},$$

for $k \in \mathbb{Z}$, $k \geq 0$, which are Hilbert spaces endowed with the inner product (and norm),

$$\langle u, v \rangle_{H_\eta^k} := \langle \eta u, \eta v \rangle_{H^k}, \quad \|v\|_{H_\eta^k}^2 := \|\eta v\|_{H^k}^2 = \langle v, v \rangle_{H_\eta^k}.$$

According to custom, we denote $H_\eta^0(\mathbb{R}; \mathbb{C}) = L_\eta^2(\mathbb{R}; \mathbb{C})$.

Let us suppose that $\lambda \in (-\infty, 0]$ is an eigenvalue associated to an eigenfunction $U = \sum U_m Y_m \in H^2(\Omega_L)$ of problem (22). Let $m \in \mathbb{Z}$, $m \geq 1$ be a single mode for which $U_m \not\equiv 0$. Consequently, $W_m \not\equiv 0$ and $\|W_m\|_{L_\eta^2} > 0$. (The modes $m \geq 1$ for which $U_m \equiv 0$ do not contribute to the energy estimate.) Then from equation (29) and Lemma 1 we have that

$$|\lambda| \int_{-\infty}^{+\infty} D(\phi) |W_m|^2 dz = \int_{-\infty}^{+\infty} D(\phi)^2 |\partial_z W_m|^2 dz + \frac{m^2}{\pi^2 L^2} \int_{-\infty}^{+\infty} D(\phi)^2 |W_m|^2 dz + J,$$

where

$$J := - \int_{-\infty}^{+\infty} D(\phi)^2 \Psi_z \partial_z \left(\frac{|W_m|^2}{\Psi} \right) dz = \int_{-\infty}^{+\infty} 2D(\phi) D'(\phi) \phi_z \frac{\Psi_z}{\Psi} |W_m|^2 dz + \int_{-\infty}^{+\infty} D(\phi)^2 \frac{\Psi_{zz}}{\Psi} |W_m|^2 dz,$$

after integration by parts.

Lemma 2. *The functions $D'(\phi) \phi_z \Psi_z / \Psi$ and $D(\phi) \Psi_{zz} / \Psi$ are uniformly bounded in $z \in \mathbb{R}$.*

Proof. Follows from the definition of Ψ , the rates of decay (17) and (18), and straightforward computations. □

In view of last lemma we have

$$|J| \leq C \int_{-\infty}^{+\infty} D(\phi) |W_m|^2 dz = C \|W_m\|_{L_\eta^2}^2,$$

for some uniform $C > 0$. Substituting back yields the estimate

$$|\lambda| \|W_m\|_{L_\eta^2}^2 \leq \left(\sup_{z \in \mathbb{R}} D(\phi) \right) \left(\|\partial_z W_m\|_{L_\eta^2}^2 + \frac{m^2}{\pi^2 L^2} \|W_m\|_{L_\eta^2}^2 \right) + C \|W_m\|_{L_\eta^2}^2.$$

This estimate holds for each fixed eigenvalue λ and all values of $m \geq 1$. It provides an upper bound for $|\lambda|$ in terms of m (recall that $|\lambda| = -\lambda > 0$, in view of Lemma (1)). Notice that the effective diffusion coefficient $D(\phi)$ (that is, the weight of the Sobolev norms) depends on the intensity of the chemotactic signal χ_0 as well. Therefore, we normalize with respect to the weighted L^2 -norm to obtain

$$|\lambda| \leq \rho_m C_m \left(\sup_{z \in \mathbb{R}} D(\phi) \right) + C, \tag{30}$$

where

$$\rho_m := \frac{\|W_m\|_{H_\eta^1}^2}{\|W_m\|_{L_\eta^2}^2} > 0,$$

and $C_m > 0$ is a constant depending on m , satisfying

$$C_m \leq C_1 + m^2 C_2,$$

for some uniform constants $C_1, C_2 > 0$.

Lemma 3. *For any $u \in H_\eta^1(\mathbb{R}; \mathbb{C})$ with $\|u\|_{L_\eta^2} > 0$, the ratio*

$$\rho = \frac{\|u\|_{H_\eta^1}^2}{\|u\|_{L_\eta^2}^2}$$

is a uniformly bounded function of $\chi_0 > 0$.

Proof. Since $D(\cdot)$ is uniformly bounded from above, it is clear that $H_\eta^k \subset H^k$ for all $k \geq 0$. The conclusion follows by noticing that both the numerator and the denominator are linear on χ_0 ,

$$\rho = \frac{\|u\|_{H_{\eta_1}^1}^2 + \chi_0 \|u\|_{H_{\eta_2}^2}^2}{\|u\|_{L_{\eta_1}^2}^2 + \chi_0 \|u\|_{L_{\eta_2}^2}^2} = O(1),$$

for all $\chi_0 > 0$ and where the weight functions η_1, η_2 are given by

$$\eta_1 = \sqrt{\sigma_0 v_0 \phi (1 - \phi / v_0)}, \quad \eta_2 = \sqrt{\sigma_0 v_0 \phi^2 (1 - \phi / v_0)}.$$

□

Therefore, estimate (30) shows that the bounds for the eigenvalues and their dependence on the intensity of the chemotactic signal are controlled by the function

$$\sup_{z \in \mathbb{R}} D(\phi) = \max_{u \in [0, v_0]} D(u) = \max_{u \in [0, v_0]} \left(\sigma_0 v_0 u \left(1 - \frac{u}{v_0} \right) (1 + \chi_0 u) \right).$$

Let

$$G(u) := u \left(1 - \frac{u}{v_0} \right) (1 + \chi_0 u), \quad u \in [0, v_0].$$

After straightforward calculations one finds that, for positive values of the chemotactic sensitivity $\chi_0 > 0$, the maximum of the cubic polynomial G on the interval $[0, v_0]$ occurs at

$$u_*(v_0, \chi_0) = \frac{1}{3} \left(v_0 - \frac{1}{\chi_0} + \sqrt{\left(v_0 - \frac{1}{\chi_0} \right)^2 + \frac{3v_0}{\chi_0}} \right) \in (0, v_0).$$

Thus, the maximum of G (and hence the energy bound for $|\lambda|$ in (30)) is controlled by

$$\Theta(v_0, \chi_0) := G(u_*(v_0, \chi_0)) = u_*(v_0, \chi_0) \left(1 - \frac{u_*(v_0, \chi_0)}{v_0} \right) (1 + \chi_0 u_*(v_0, \chi_0)).$$

By standard calculus tools, one easily verifies that, for fixed values of the initial nutrient concentration v_0 , the bound Θ is an increasing function of the chemotactic signal $\chi_0 \geq 0$. Figure 2 shows this behaviour of Θ as a function of χ_0 , for different fixed values of $v_0 = 0.5, 0.75, 1.0, 1.5$.

Whence, in view of Lemma 1 and (30), we have

$$0 > \lambda > -(C + \rho_m C_m \sigma_0 v_0 \Theta(v_0, \chi_0)). \tag{31}$$

The right hand side of (31) is a negative, decreasing function of $\chi_0 \in (0, +\infty)$ for each fixed value of the nutrient level v_0 . In lay terms, this shows that for greater values of $\chi_0 \geq 0$, the eigenvalues of the linearized operator around the front are allowed to be more negative. Since λ is actually the in-time growth rate of perturbations of the form $w = e^{\lambda t} U$, this suggests that λ is further pushed to the negative side as the chemotactic signal is increased, delaying the formation of unstable patterns (fingering) around the envelope front. To sum up, although the envelope front moves faster due to chemotaxis, the spectral bounds for the eigenvalues of the linearized problem actually decrease as functions of the chemotactic sensitivity χ_0 , demanding greater energy to make the patterns transversally unstable. Finally, it is to be observed that our estimation is elementary, in spite of working with a density-dependent, degenerate, nonlinear diffusion coefficient.

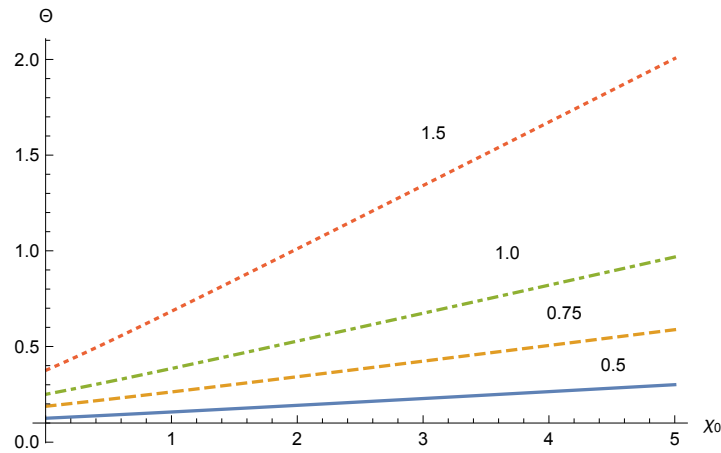


Fig. 2 Plot of $\Theta(v_0, \chi_0)$ as a function of $\chi_0 \geq 0$ for different fixed values of $v_0 = 0.5, 0.75, 1.0, 1.5$ (color plot online).

4 Discussion

In this paper we have shown that, for a generic nonlinear, degenerate cross-diffusion, chemotactic model of the form (10), underlying balanced kinetic terms, and under the assumptions of approximately constant chemotactic sensitivity, together with a scalar conservation law approximation that is suggested by the balanced source/loss terms, envelope traveling fronts (which are, at first order, locally planar in space) are spectrally stable under transversal perturbations. More precisely, the eigenvalues associated to the perturbations in both space dimensions are real and non-negative. This is shown using an appropriate change of variables and by performing energy estimates on the perturbation (spectral) equations. These energy estimates provide, in addition, bounds for the eigenvalues of the linearized operator around the front. Elementary calculations show that these bounds decrease as functions of the chemotactic sensitivity $\chi_0 \geq 0$, suggesting that, as χ_0 grows, the patterns are more stable.

Of course, these observations apply to a first order approximation of the general problem. The crucial approximation is to recast the stability problem of the front as an equivalent one for an effective scalar equation. This is possible thanks to the balanced terms of production of bacterial cells and loss of nutrient concentration, which induce a conservation law for the total density. As a consequence, the resulting effective nonlinear density-dependent diffusion coefficient for a scalar reaction-diffusion equation of Fisher-KPP type is also dependent on the chemotactic sensitivity parameter, pushing the interface to be deformable on shorter scales than the new diffusion length as the chemotactic signal is increased.

Our quantitative observations are consistent with the analysis of Arouh and Levine [2], who showed that chemotaxis suppresses the instability of fronts for a Kessler-Levine system with constant diffusivities and nutrient chemotactic terms. Their analysis applies to balanced source/loss kinetic terms of cut-off type. It is to be observed that the method employed here is elementary and applicable to density-dependent diffusion coefficients. In contrast, the method of Arouh and Levine applies (apparently) to constant diffusion models only, as they compute asymptotic expansions of the eigenvalues of the Laplace operator. Both theirs and our results show the suppression of colony branching when the bacteria are assisted chemotactically toward nutrients, a fact that has been confirmed numerically in other systems, such as models for the aggregation of *Paenibacillus dendritiformis* (see, e.g., [22]) containing balanced kinetic terms as well.

This stabilizing effect of chemotaxis appears to contradict the results of Funaki *et al.* [7], which show that when the chemotactic signal is present traveling front solutions are destabilized. Indeed, the authors actually show that the transversal instability depends upon wave numbers which, as they increase, produce unstable eigenvalues of a linearized problem, provided that the chemotactic sensitivity function is uniformly convex. The

model considered by Funaki and collaborators, however, is a reaction-diffusion-chemotaxis system for which the production and degradation terms are not balanced (unlike those in (10) and in the systems considered in [2,22]). These reaction terms modify the form of the linearized operator around the wave and hence, its stability. It is well known that balanced kinetic terms cause stable wave pinning, even in the case of reaction-diffusion systems without chemotaxis (see, for example, [17]). Therefore, we conjecture that this robustness is lost in the system studied by Funaki and collaborators, causing branching instabilities.

Acknowledgements

The research of RGP was supported by DGAPA-UNAM, grant PAPIME PE-104116.

References

- [1] J. Adler, (1966), *Chemotaxis in bacteria*, Science 153 no. 3737, pp. 708–716.
- [2] S. Arouh and H. Levine, (2000), *Nutrient chemotaxis suppression of a diffusive instability in bacterial colony dynamics*, Phys. Rev. E 62 no. 1, pp. 1444–1447.
- [3] E. Ben-Jacob, I. Cohen, and H. Levine, (2000), *Cooperative self-organization of microorganisms*, Advances in Physics 49, no. 4, pp. 395–554.
- [4] J. A. Butanda, (2016), *Spectral methods in the study of reaction-diffusion traveling fronts*. (In Spanish.) M.Sc. Thesis, Universidad Nacional Autónoma de México.
- [5] I. Cohen, A. Czirók, and E. Ben-Jacob, (1996), *Chemotactic-based adaptive self organization during colonial development*, Phys. A 233, no. 3–4, pp. 678–698.
- [6] R. A. Fisher, (1937), *The wave of advance of advantageous genes*, Annals of Eugenics 7, pp. 355–369.
- [7] M. Funaki, M. Mimura, and T. Tsujikawa, (2006), *Travelling front solutions arising in the chemotaxis-growth model*, Interfaces Free Bound. 8, no. 2, pp. 223–245.
- [8] I. Golding, Y. Kozlovsky, I. Cohen, and E. Ben-Jacob, (1998), *Studies of bacterial branching growth using reaction-diffusion models for colonial development*, Phys. A 260, no. 3–4, pp. 510–554.
- [9] K. Kawasaki, A. Mochizuki, M. Matsushita, T. Umeda, and N. Shigesada, (1997), *Modeling spatio-temporal patterns generated by Bacillus subtilis*, J. of Theor. Biol. 188, no. 2, pp. 177 – 185.
- [10] E. F. Keller and L. A. Segel, (1971), *Model for chemotaxis*, J. Theor. Biol. 30, no. 2, pp. 225 – 234.
- [11] E. F. Keller and L. A. Segel, (1971), *Traveling bands of chemotactic bacteria: A theoretical analysis*, J. Theor. Biol. 30, no. 2, pp. 235 – 248.
- [12] A. N. Kolmogorov, I. Petrovsky, and N. Piskunov, (1937), *Etude de l'équation de la diffusion avec croissance de la quantité de matière et son application à un problème biologique*, Mosc. Univ. Bull. Math 1, pp. 1–25.
- [13] R. I. Lapidus and R. Schiller, (1976), *Model for the chemotactic response of a bacterial population*, Biophys. J. 16, no. 7, pp. 779–789.
- [14] J. F. Leyva, C. Málaga, and R. G. Plaza, (2013), *The effects of nutrient chemotaxis on bacterial aggregation patterns with non-linear degenerate cross diffusion*, Phys. A 392, no. 22, pp. 5644–5662.
- [15] J. F. Leyva and R. G. Plaza, (2016), *Spectral stability of traveling fronts for reaction diffusion-degenerate Fisher-KPP equations*. Preprint. <https://arXiv:1606.04831>.
- [16] L. Malaguti and C. Marcelli, (2003), *Sharp profiles in degenerate and doubly degenerate Fisher-KPP equations*, J. Differential Equations 195, no. 2, pp. 471–496.
- [17] Y. Mori, A. Jilkine, and L. Edelstein-Keshet, (2011), *Asymptotic and bifurcation analysis of wave-pinning in a reaction-diffusion model for cell polarization*, SIAM J. Appl. Math. 71, no. 4, pp. 1401–1427.
- [18] M. Ohgiwari, M. Matsushita, and T. Matsuyama, (1992), *Morphological changes in growth phenomena of bacterial colony patterns*, J. Phys. Soc. Jpn. 61, no. 3, pp. 816–822.
- [19] F. Sánchez-Garduño and P. K. Maini, (1994), *Existence and uniqueness of a sharp travelling wave in degenerate non-linear diffusion Fisher-KPP equations*, J. Math. Biol. 33, no. 2, pp. 163–192.
- [20] F. Sánchez-Garduño and P. K. Maini, (1997), *Travelling wave phenomena in non-linear diffusion degenerate Nagumo equations*, J. Math. Biol. 35, no. 6, pp. 713–728.
- [21] D. Schwarcz, H. Levine, E. Ben-Jacob, and G. Ariel, (2016), *Uniform modeling of bacterial colony patterns with varying nutrient and substrate*, Phys. D 318/319, pp. 91–99.
- [22] L. J. Tucker, (2010), *A new computational approach to simulate pattern formation in Paenibacillus dendritiformis bacterial colonies*, PhD thesis, University of California, San Diego. <https://escholarship.org/uc/item/6x91c78r>.

- [23] G. H. Wadhams and J. P. Armitage, (2004), *Making sense of it all: bacterial chemotaxis*, *Nature Rev. Molecular Cell Biol.* 5, no. 12, pp. 1024–1037.
- [24] J.-I. Wakita, K. Komatsu, A. Nakahara, T. Matsuyama, and M. Matsushita, (1994), *Experimental investigation on the validity of population dynamics approach to bacterial colony formation*, *J. Phys. Soc. Jpn.* 63, no. 3, pp. 1205–1211.

©UP4 Sciences. All right reserved.